Non-Newtonian and Gas-non–Newtonian Liquid Flow through Elbows – CFD Analysis

T. K. Bandyopadhyay[1] and S. K. Das[2†]

[1]Chemical Engineering Department, National Institute of Technology, Agartala
[2]Chemical Engineering Department, University of Calcutta, 92 A. P. C. Road, Kolkata – 700 009, India

†*Corresponding Author Email: drsudipkdas@vsnl.net*

ABSTRACT

Computational Fluid Dynamics (CFD) analysis for the flow of non-Newtonian and gas-non-Newtonian liquid through elbows is presented. The commercial software Fluent 6.3 has been used for the simulation. Laminar non-Newtonian pseudoplastic power law model has been used for the simulation of non-Newtonian liquid flow through elbows. For two-phase flow Elurian-Elurian approach has been used for simulation. The CFD analysis have been tested from our previously published experimental results, Bandyopadhyay and Das (2007), Bandyopadhyay et al. (2000).

NOMENCLATURE

CFD	computational fluid dynamics
d	tube diameter (m)
g	acceleration due to gravity (m/s^2)
G	generation of turbulent kinetic energy (J/m^3 s)
K	momentum exchange coefficient (kg/m^{3}s)
K$^/$	consistency index (NS^{n}m^{-2})
m	mass transfer rate (kg/m^{3}s)
n	number of phases
n$^/$	flow behavior index (dimensionless)
$\vec{R}$	interaction force (N/m^3)
Re	Reynolds number (dimensionless)
t	time (s)
u	velocity (m/s)

Greek Symbols

α	Volume fraction (dimensionless)
ρ	Density (kg/m^3)
μ_{eff}	effective viscosity (Ns/m^2)
P	pressure (kPa)
τ	shear stress (N m^{-2})

Subscripts

c	curvature
g	gaseous state
p, q	phase
p	pressure
eff	effective

1. INTRODUCTION

Pipe fittings like valves, bends, elbows, tees, reducers, expander etc. are the integral part of any piping system. Flow through piping components are more complex than the straight pipes. The problem of determining the pressure losses in elbows is important in design and analysis of the fluid machinery. Forcing a fluid through elbow consumes energy provided by the drop in pressure across the elbow. The friction between the fluid and the fitting wall causes this pressure drop. Researchers (Edwards *et al*. 1985; Das

et al. 1991; Banerjee *et al.* 1994; Bandyopadhyay and Das 2007) reported experimental studies of non-Newtonian liquid flow through various piping components and empirical correlation were suggested for individual piping components. However, data or equations for pressure drops through elbows are meager. Since most non-Newtonian liquids are highly viscous in nature and the laminar flow is of greatest practical interest (Das *et al*. 1989).

Two-phase gas-liquid flow through elbows is much more complex in nature. When flow enters the curved portion, the heavier density phase is subjected to a large centrifugal

force, which causes the liquid to move away from the centre of curvature. Studies on the effect of curve geometry on two-phase gas-liquid flow are sporadic in the literature Das *et al*. (1992); Banerjee and Das (1998); Bandyopadhyay *et al*. (2000) reported the experimental investigation for gas-non-Newtonian liquid flow through bends, valves and elbows. They developed empirical correlation for predicting the frictional pressure drop across the piping components. In order to achieve optimum performance, an accurate design technique is necessary for the prediction of the pressure drop for non-Newtonian and gas-non-Newtonian liquid through elbows.

Computational fluid dynamics (CFD) is the science of predicting fluid flow, heat and mass transfer, chemical reaction and related phenomena by solving numerically by the set of governing mathematical equations along with the conservation of mass, momentum, energy. The results of CFD analysis are relevant in conceptual studies of new designs, detailed product development, troubleshooting in existing unit and redesign. The CFD analysis complements testing and experimentation which reduces the total effort required in experimental design and data acquisition.

Computational Fluid Dynamics (CFD) can serve to evaluate the frictional pressure losses in piping systems, secondary flow effects can be visualized to aid in better understanding of the flow phenomena and can be applied to piping design for the improvement of the flow characteristics. However CFD analysis often requires fine tuning by comparison with the reliable experimental data. Edwards *et al*. (1998) developed a CFD based model to predict erosion in piping system for slurry pipeline. Hidayat and Rasmuson (2002) reported the numerical simulation of gas-solid flow in a U-bend. Etemad and Sunden (2004) studied numerical analysis of turbulent

convective heat transfer in a square–sectioned U-bend duct. Marn and Ternik (2006) numerically studied the laminar flow of shear-thickening electrostatic ash-water mixture through a 90° pipe bend. Numerical simulations are performed for the dilute gas-solid flow through rectangular duct containing a horizontal to vertical bend of 90° angle by Kuan *et al*. (2003). Brown (2006) reported the causes of highly localized erosion in slurry pipeline in an aluminium refinery through CFD and subsequently developed the newer design of the pipeline. Saha and Jain (2008) used CFD analysis for slurry pipeline to investigate the erosion in the pipeline. Wu and Chen (2008) used commercial CFD code to simulate the flow fields of lab-scale, scale-up and pilot-scale anaerobic digesters. Their simulated results were validated against the experimental data from literature using liquid as Newtonian and non-Newtonian in nature. Manzar and Shah (2009) reported the CFD analysis for straight and coils tubes using different Newtonian and non-Newtonian liquids. In this paper commercial CFD packages Fluent 6.3 is used to predict the pressure drop across the elbows for non-Newtonian and gas-non-Newtonian liquid flow through elbows. CFD analysis tested with our previous experimental results by Bandyopadhyay and Das (2007); Bandyopadhyay *et al*. (2000).

2. EXPERIMENTS

Details of the experimental investigation for non-Newtonian and gas-non-Newtonian liquid flow through elbows are reported in our earlier work published by (Bandyopadhyay and Das 2007; Bandyopadhyay *et al*. 2000). The ranges of variables investigated are shown in Table 1.

Table 1 Range of variables

Measurement Type	Range
Liquid and Flow properties	
Concentration of SCMC Solution (kg/m^3)	0.2 to 0.8
Flow behavior index	$0.6015 \leq n^/ \leq 0.9013$
Consistency index ($Ns^{n'}/m^2$)	$0.0142 \leq K^/ \leq 0.7112$
Density (kg/m^3)	$1001.69 \leq \rho \leq 1003.83$
Liquid Flow Rate $Q_l \times 10^5 (m^3/s)$	3.75 to 29.83
Gas Flow Rate $Q_g \times 10^5 (m^3/s)$	2.90 to 44.75
Reynolds Number	$47.51 \leq R_e \leq 2234.21$
Dean Number	$32.41 \leq D_e \leq 2130.23$
Pressure Drop (Experimental) (kPa)	$0.1333 \leq \Delta P \leq 45.46$
Elbow	
Angle of Elbow	45° to 135°
45^0 elbow	Radius of curvature = 0.011m Linear length of the elbow = 0.014m
90^0 elbow	Radius of curvature = 0.022m Linear length of the elbow = 0.011m
135^0 elbow	Radius of curvature = 0.017m Linear length of the elbow = 0.016m

3. MATHEMATICAL MODEL

3.1 Single Phase

Dilute solution of SCMC follows the non-Newtonian pseudoplastic Power law model. In general for non-Newtonian liquids the effective viscosity is used for calculation and defined as,

$$\mu_{eff} = K' \left(\frac{8u}{d}\right)^{n'-1} \tag{1}$$

The governing equation is the Navier–Stokes equation as,

$$\rho \frac{\partial u}{\partial t} + \rho u.\nabla u = \mu_{eff} \nabla^2 u - \nabla P \tag{2}$$

and the continuity equation is

$$\nabla u = 0 \tag{3}$$

Where,

$$\nabla = i \frac{\partial}{\partial x} + j \frac{\partial}{\partial y} + k \frac{\partial}{\partial z} \tag{4}$$

As the flow of liquid is laminar in all cases the viscous model, i.e., laminar non-Newtonian Power Law model is used for the CFD analysis. These equations are solved subject to the following boundary conditions,

(i) The elbow walls are assumed rigid and a no-slip condition is imposed.

(ii) At the outlet, the velocities are free but the normal and tangential stresses are constrained to be zero and the gauge pressure is set to zero.

(iii) At the inlet, a uniform velocity profile is used with a time varying forcing function which represents the flow in the left portion of elbows.

3.2 Two-Phase

Two-phase flow was modeled with the Eulerian-Eulerian approach, where the phases are assumed to be interpenetrating continua. One of the phases defined as continuous and the other as dispersed, the phases sum up to the unity. The pressure and gravity vectors are shared by both phases, whereas other variables are phase specific. The only notable change to the one phase solution is the presence of interfacial forces.

This model is the most general and the most complex among all the models of multi – phase flow. The substance of each phase is assumed to form continuous medium. Its motion is simulated with own system of Navier–Stokes equations, continuity equation and energy equation. According to this model, the equations written for each phase are solved jointly. At high values of α_g , the dispersed particles strongly influence the carrier flow, and only the multi – phase Eulerian model should be used for adequate simulation of such flows.

Continuity equation

$$\frac{\partial}{\partial t} \alpha_q \rho_q + \nabla.\left(\alpha_q \rho_q u_q\right) = \sum_{p=1}^{n} m_{pq} \tag{5}$$

where α_q = fraction for the q-th phase

Momentum for q-th phase

$$\frac{\partial}{\partial t}\left(\alpha_q \rho_q u_q\right) + \nabla.\left(\alpha_q \rho_q u_q u_q\right) = -\alpha_q \nabla p + \alpha_q \rho_q g$$
$$+\nabla.\overline{\overline{\tau_q}} + \sum_{p=1}^{n}\left(R_{pq} + m_{pq}u_q\right) + \alpha_q \rho_q \left(F_q + F_{lift,q} + F_{vm,q}\right) \tag{6}$$

The inter-phase exchange forces are expressed as,

$$R_{pq} = K_{pq}\left(u_p - u_q\right) \tag{7}$$

where K_{pq} = fluid-fluid exchange coefficient

As the flow of liquid is laminar, non-Newtonian Power Law model is used as viscous model and Eulerian model is used as multiphase model for the CFD analysis.

3.3 CFD Procedure

Geometries for the straight pipe, elbows are created in Gambit 6.3 preprocessor. A typical mesh has about 4×10^3–3×10^4 order unstructured tetrahedral mesh for elbows are used. Inlet and outlet are located at each end of the elbows. The inlet is used to specify the inlet velocity and outlet is used to specify pressure outlet. These geometries of the elbows are imported into Fluent 6.3 in a Cartesian co-ordinate system. Fluent 6.3 solved the governing equations in 3-D geometry. Laminar non-Newtonian Power Law model have been used for simulation. The model solves for Navier-stokes equation at prescribes velocities. The governing equations are non linear and several iterations of loop must be performed before a convergent solution is obtained. The first-order upwind scheme is used in the discretization of set of governing equations, standard interpolation schemes is used for calculating cell-face pressures for using the Segregated solver in Fluent 6.3. Pressure-velocity coupling refers to the numerical algorithm which uses a combination of continuity and momentum equations to derive an equation for pressure (or pressure correction) when using the segregated solver. Simple algorithm is used in Fluent 6.3 domain.

The general procedure to simulate SCMC flow through elbows based on Gambit 6.3 and Fluent 6.3 software is outlined below,

1. Perform meshing under Gambit 6.3 :

   ➢ Create a computational domain at the flow region,

   ➢ The grids were generated using t-grid (tetrahedral) meshes,

   ➢ Controlling a smooth change in the mesh size by size functions,

   ➢ Specify boundary and continuum types,

   ➢ Examine the mesh to ensure that the high skewness is below 0.9 for tetrahedral meshes.

2. Import the mesh file to Fluent 6.3 and check the mesh.

3. Define a 3-D, unsteady, implicit, and pressure-based solver.

4. Activate the single phase laminar non-Newtonian power law model and Eulerian laminar non-Newtonian power law multiphase model.

5. Define a laminar non-Newtonian power law model for single phase and a Eulerian laminar model for multiphase. Slip velocity is added.

6. Enable the SCMC properties with laminar flow conditions using the text command - define/models/viscous/laminar. Putting the non-Newtonian fluid values - flow behavior index, consistency index, temperature and effective viscosity values at the inlet velocity.

7. Define the phases by setting SCMC as the primary phase and gas as the secondary phase, and keeping the default selection of Schiller-Naumann drag model in the phase interaction panel.

8. Define the operating conditions by turning on gravity and specify the operating density.

9. Solution control methodology – Under relaxation factors – 0.5 for pressure, 0.3 for momentum, 0.1-0.9 for volume fraction, and default values for the other parameters. Standard schemes – STANDARD for momentum and volume fraction, and 1st order upwind for other variables. Pressure-velocity SIMPLE coupling used;

10. Initialize the solution – velocity; Enable the plotting of residuals during the calculation, and kept the default convergence criteria, 1×10^{-3} for continuity and 1×10^{-5} all residuals.

3.4 Assumptions for air-SCMC flow through elbow

The following concepts and assumptions were made,

1. The solution temperature is constant at 30^{0}C, and each phase is an isothermal and incompressible fluid;

2. A single pressure is shared by both phases;

3. Momentum and continuity equations are solved for each phase;

4. Our system behaves like a plug and slug flow regimes. But we assumed two-phase flow as a bubbly flow due to simplicity of calculation in which SCMC is treated as the primary phase while gas is treated as the secondary phase;

5. The secondary phase consists of uniform and unchanging bubbles dispersed in a continuous phase;

6. The bubbles size is assumed to be small, 0.1mm spherical in size;

7. Two–phase Eulerian laminar non-Newtonian power law model is used;

8. Physical properties are uniform throughout;

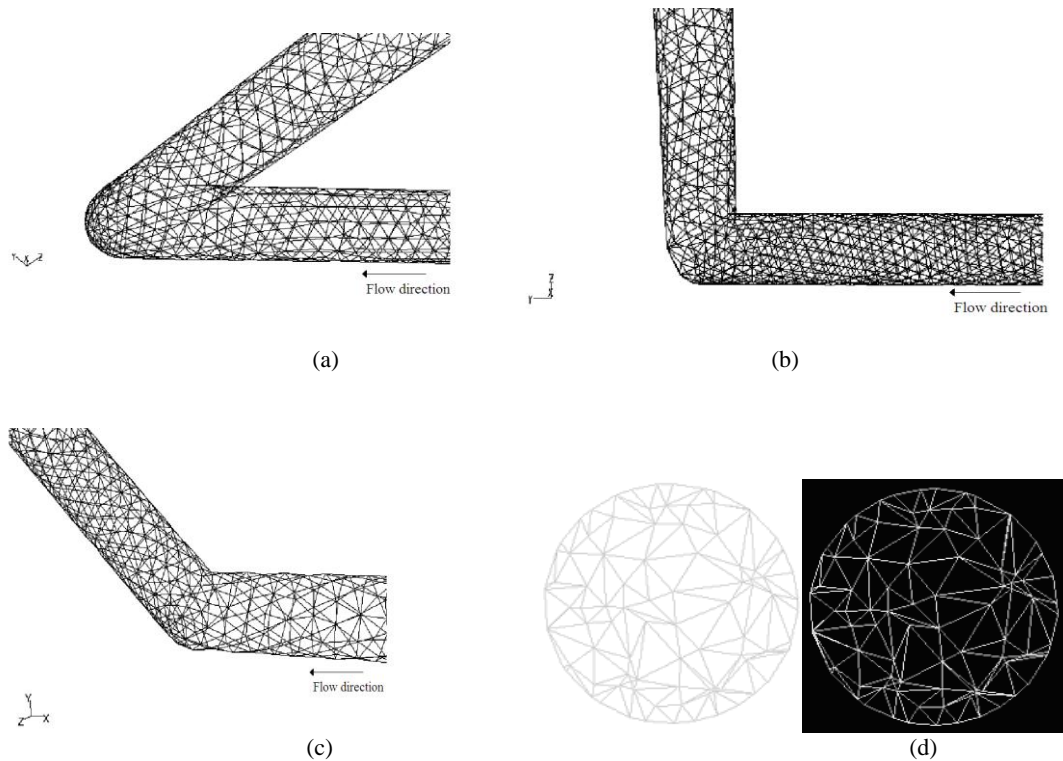9. Different phases move at different velocities (slip velocities);

10. The drag force from SCMC phase acting on the gas bubbles is included into the interphase momentum exchange;

11. There are no external body force and virtual mass force, and the effect of lift force on the bubbles is negligible.

4. RESULTS AND DISCUSSION

4.1 Criteria for Convergence and Grid Independency

The convergence criterions were set at 10^{-5} for all equations except for the transport equation which residual was set at 10^{-3}. A computational domain L≥200D was used to ensure fully developed flow results could be obtained for all elbows. In general the final results depend upon mesh geometries. Subsequent decrement and increment in mesh resolution by 50% were applied to evaluate if the employed mesh resolution was adequate to obtain accurate solutions. It was observed that when the mesh resolution was decreased by 50% the axial velocity profile was 7-12% of the currently employed mesh velocity profile for elbows. As the present mesh resolution was increased by 50% the axial velocity profile changes 1-3% for elbows. These results suggest that the current mesh resolution is sufficient to obtain grid independent solutions for the proposed model.

4.2 Non-Newtonian Liquid Flow Through Elbows

Fig. 1 shows the mesh generated for different elbows. Unstructured tetrahedral grid is fitted well for the cases of elbows due to its curved structure. As the fluid flows through the straight pipe and then enter into the elbow section, the pressure which is uniform across the flow in the straight section, must adjust in the elbow to counter the centrifugal force. The pressure is greatest at the outer wall furthest from the centre of curvature and least at the inner wall nearest to the centre of curvature. At the inlet of the elbow a low pressure exists in the inner wall and high pressure exists at the outer wall, it is clearly indicated in Fig. 2. This initial pressure gradient resulting from the change from straight to curve flow, a cross stream pressure gradient exists in the elbow, at the elbow inlet the boundary layer on the outer wall experiences the effect of an the adverse stream wise pressure gradient which may be sufficiently strong for 45^{0} elbow than compare to 135^{0} elbow and produce local separation and the inner wall boundary layer is accelerated (Fig. 3). The reverse occurs at the exit of the elbow where local pressure gradients of the opposite sign appear as the flow adjust to uniform pressure condition of the downstream. The impacts of the curve geometry into the straight section were extended 5 pipe diameter upstream of the elbow and also 5 pipe diameter downstream of the elbow. This impact depends on the velocity of the flow and also the elbow angle and effect is maximum for the 45^{0} elbow and minimum for the 135^{0} elbow. Thus the flow at the entrance of the elbow differs considerably from a fully developed pipe flow. The flow in elbow is influenced by centrifugal force due to its curvature.

(a)

(b)

(c)

(d)

Fig. 1. Unstructured Tetrahedral grid
(a) 45^0 elbow - Grid Size: No. of cells = 25985; No. of faces = 57149, No. of nodes = 7310
(b) 90^0 elbow - Grid Size: No. of cells = 29157; No. of faces = 64167, No. of nodes = 8208
(c) 135^0 elbow -Grid Size: No. of cells = 4427; No. of faces = 9778, No. of nodes = 1279
(d) Tetrahedral grid for selected plane of the elbow

This centrifugal force is, in principle, balanced by a pressure gradient in the plane of curvature. However, near the wall where the velocity is small, this pressure gradient can no longer be balanced and consequently fluid in the middle of the pipe moves at the outer wall and then turns to move inward along the wall. The flow on the outer wall and separation at the inner wall make flow very complex (Fig. 4). The result is a secondary flow superimposed in the main flow in the plane perpendicular to the main flow. The magnitude and direction of the flow depends on Dean number ($\mathrm{Re}\sqrt{\dfrac{d}{d_c}}$). The direct effect of secondary flow is to displace the region of maximum velocity to the centre towards the outer wall. For the elbow entrance the mean axial velocity profile significantly altered with respect to the fully developed profile in the straight pipe and the location of the maximum velocity is shifted towards the inner wall of the elbow. This explained by the fact that no centrifugal forces due to redirection of flow are present at the entrance of the flow.
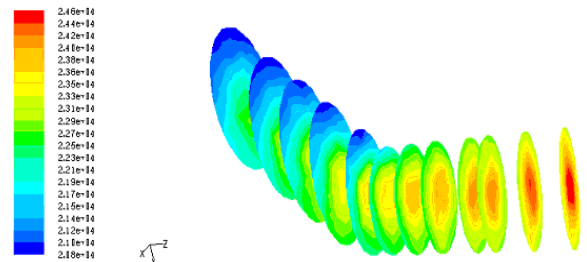

Fig. 2. Contour plot of total pressure inside the different points of 135^0 elbow SCMC Conc. (kg/m^3): 0.8, Liquid flow rate, Q_l (m^3/s): 21.94x10^{-5}
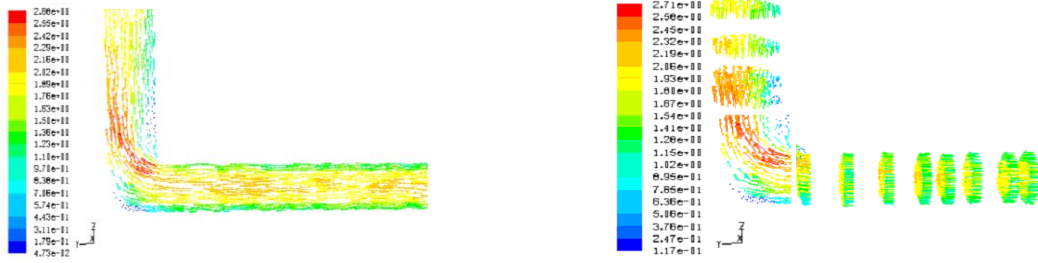
Fig. 3. Contour plot of velocity vector inside the different points of 90^0 elbow
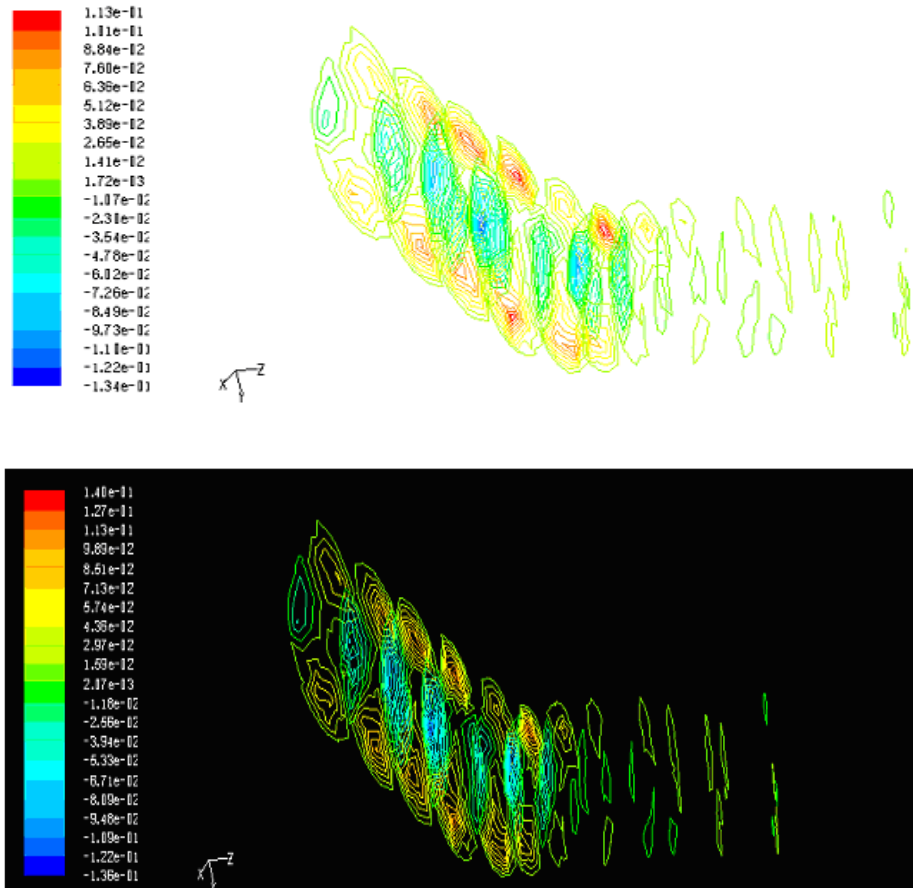SCMC Conc. (kg/m^3): 0.8, Liquid flow rate, Q_l (m^3/s): 21.94x10^{-5}

Fig. 4. Contour plot of axial velocity inside the different points of 135^0 elbow
SCMC Conc. (kg/m^3): 0.8, Liquid flow rate, Q_l (m^3/s): 21.94x10^{-5}

The flow in the elbow is always developing in nature in which the velocity distributions do not attain other forms that are more or less independent of the position along the pipe axis. For 45^0 elbow exist the axial velocity moves further towards the outer radius. The secondary motion can be seen clearly in the Fig. 4. At the elbow entrance the centrifugal forces are very weak to balance the pressure gradient which results in an inward flow. With increasing deflection that is flow through inside the elbows the centrifugal forces increases and counter rotating vortices that circulate in the outer direction in the central part of the pipe (Fig. 4). This effect is more pronounced in the case of 45^0 elbow than compare to the other elbows. As the flow passes to the elbow this vortices shifted towards the inner wall and then the static pressure starts to deviate from steady value within 5 pipe diameter in the upstream of the inlet of the elbows, depending on the flow rate. In the downstream of the elbows, the pressure recovery lengths were found to be within 5 pipe diameter for all elbows, depending on the flow rate. Similar results were obtained by other researchers (Kuan *et al.* 2003; Berrouk and Laurence 2008; Kumar *et al.* 2008; Zhang *et al.* 2010). Fig.

5 shows the contours plot of static pressure. As the fluid flows through the straight pipe and then enter into the elbow section, the pressure which is uniform across the flow in the straight section, must adjust in the elbow to counter the centrifugal force. The pressure is greatest at the outer wall furthest from the centre of curvature and least at the inner wall nearest to the centre of curvature. At the inlet of the elbow a low pressure exists in the inner wall and high pressure exists at the outer wall, it is clearly indicated in Fig. 5. This initial pressure gradient resulting from the change from straight to curve flow, a cross stream pressure gradient exists in the elbow, at the elbow inlet the

boundary layer on the outer wall experiences the effect of an the adverse stream wise pressure gradient which may be sufficiently strong for 45^0 elbow than compare to 135^0 elbow. Fig. 6 shows comparison plot of experimental and CFD for 45^0 elbow. Fig. 7 shows the comparison plot of experimental pressure drop and CFD simulated data across the 135^0 elbow with liquid flow rate. Fig. 8 shows that comparison plot of the predicted pressure drop and experimental pressure drop across the elbows. In both cases experimental results matches well with the CFD simulated results.
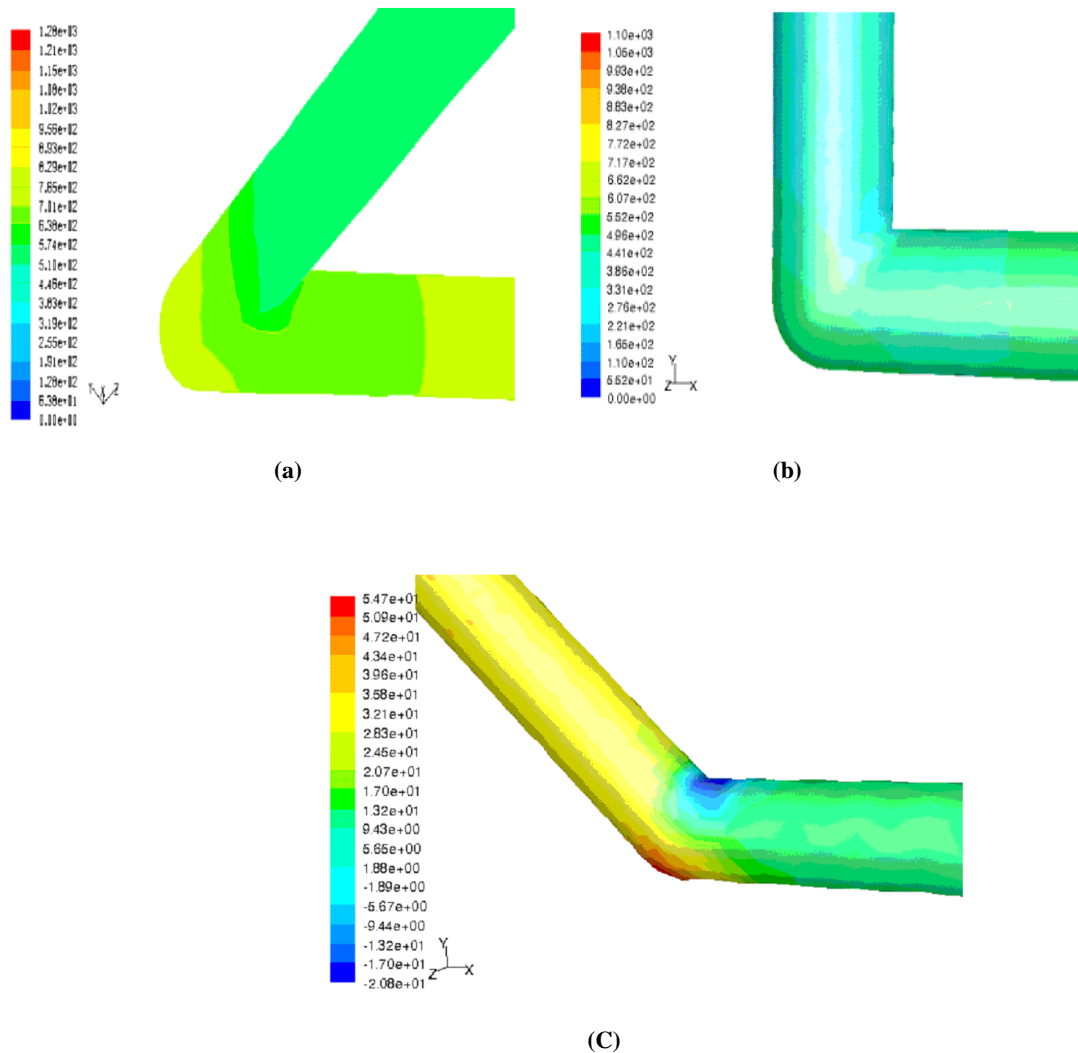

(a)

(b)

(C)

Fig. 5. Contour plot of static pressure
(a) 45^0 elbow - Concentration of SCMC solution (kg/m³): 0.2, Liquid velocity (m/s): 0.296
(b) 90^0 elbow - Concentration of SCMC solution (kg/m³): 0.2, Liquid velocity (m/s): 0.296
(c) 135^0 elbow - Concentration of SCMC solution (kg/m³): 0.2, Liquid velocity (m/s): 0.296
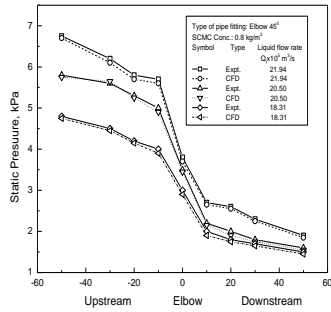
Fig. 6. Comparison plot of experimental and CFD for 45^0 elbow
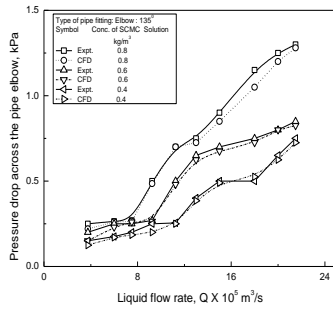

Fig. 7. Variation of pressure drop across the 135^0 elbow with liquid flow rate
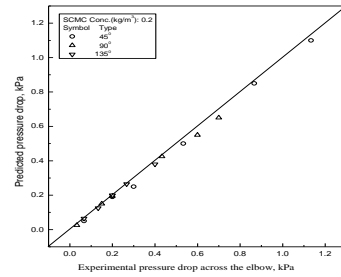

Fig. 8. Comparison plot of the predicted pressure drop and experimental pressure drop across the elbows

4.3   Gas Non-Newtonian Liquid Flow Through Elbows

Fig. 9 (a-c) shows that contour plot of velocity at different points in the elbows. It is clear from these figures that the mixture velocity is higher at the centre position and inner side of the elbow and lowers at the outer wall. As the mixture enters to the elbows due to centrifugal action heavier density phase that is liquid moves to the outer wall and lower density phase, air moves to the inner wall. Fig. 10 illustrates that the air velocity at the inner wall is higher and practically zero at the outer wall. The inlet flow regime is intermittent in nature (plug and slug). At inlet the existence of air is at the top. Due to slip exist between the liquid and air and the existence of the pressure gradient across the cross-section air velocity increases compare to the liquid velocity, due to centrifugal action the liquid is shifted towards the outer wall and a stratified flow condition attaint within the elbows.
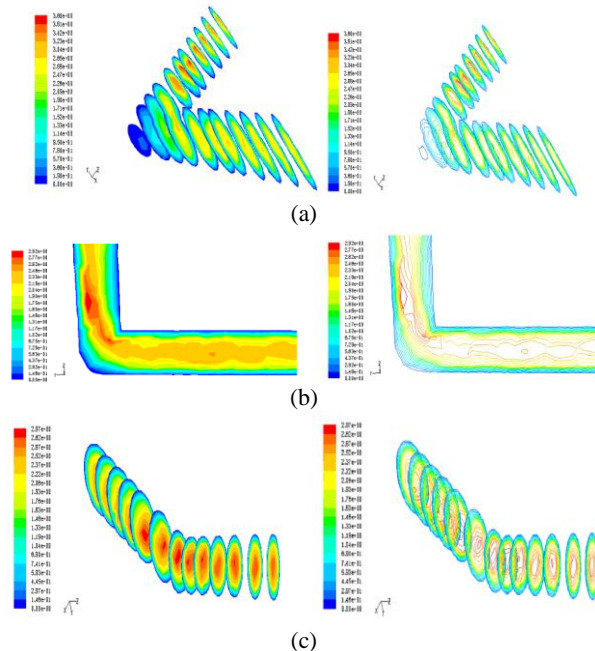

(a)

(b)

(c)

Fig. 9. Contour plot of velocity in the air-SCMC mixture at different points of elbows
SCMC concentration (kg/m^3): 0.8, SCMC velocity (m/s): 1.733
(a) 45^0, gas velocity (m/s): 3.167, gas fraction, α_g : 0.64
(b) 90^0, gas velocity (m/s): 2.3933, gas fraction, α_g : 0.58
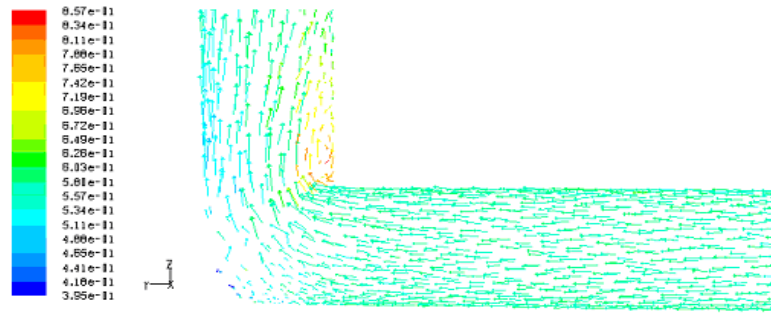(c) 135^0, gas velocity (m/s): 2.867, gas fraction, α_g : 0.62

Fig. 10. Contour plot of velocity vector for air in the mixture at different points in 90^0 elbow
SCMC concentration (kg/m^3): 0.8, SCMC velocity (m/s): 1.733,
gas velocity (m/s): 2.3933, gas fraction, α_g : 0.58

The 45° elbow shows higher pressure drop than comparing with the other elbows and it is due to faster dispersion of rope and a shorter developing flow exist. Fig. 11 shows that contour plot of static pressure at different points in the elbows. It shows that pressure is high at outer wall as heavie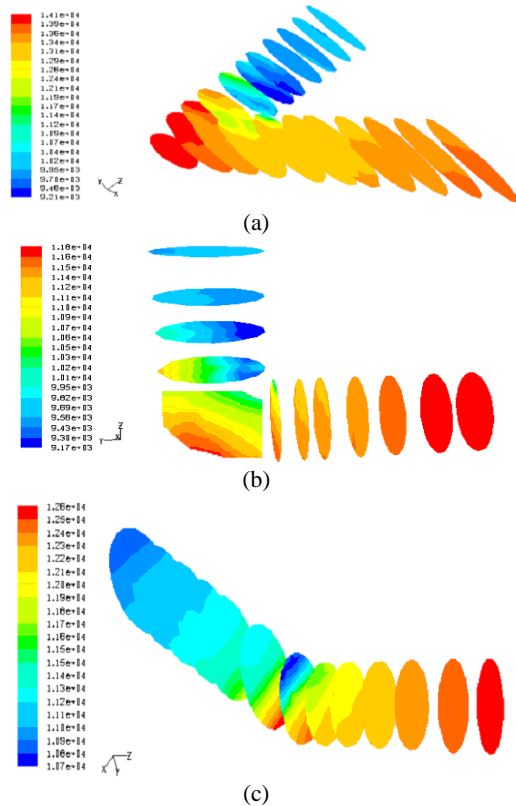r density liquid phase goes to outer wall due to centrifugal force and low at the inner wall when the air phase exists. Due to this pressure gradient at any cross section of the elbow the air is accelerated more than the liquid phase. Due to this acceleration maximum velocity is shifted for the mixer.

The secondary flow originated in a pair of counter rotating vortices at the just inside of the elbow. These vortices continue up to the downstream of the elbow, merged in the just outlet of the elbow and downstream flow return slowly to the steady state.

Fig. 12 shows that volume fraction of the SCMC and air at different point in the 90^0 elbow. It shows that heavier density phase SCMC goes to outer wall side and lighter air goes to inner wall side due to centrifugal force.
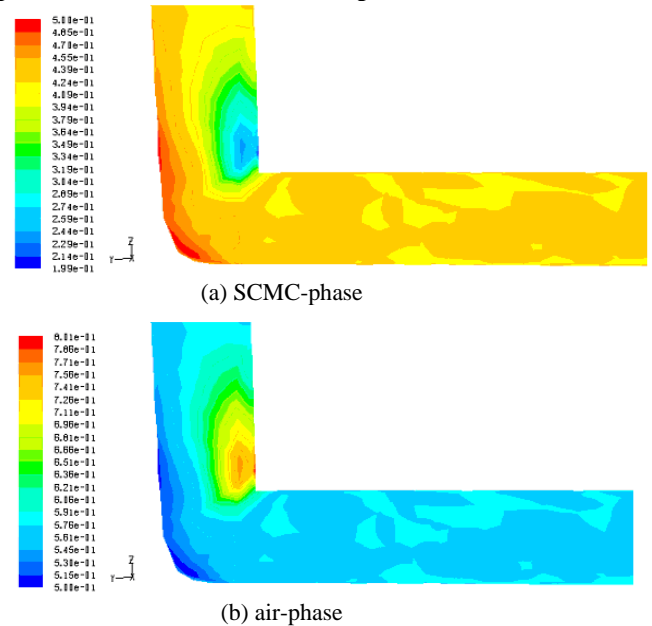

(a)

(b)

(c)

Fig. 11. Contour plot of static pressure, at different points in the elbows
SCMC concentration (kg/m^3): 0.8, SCMC velocity (m/s): 1.733

(a) 45^0, gas velocity (m/s): 3.167, gas fraction, α_g : 0.64

(b) 90^0, gas velocity (m/s): 2.3933, gas fraction, α_g : 0.58

(c) 135^0, gas velocity (m/s): 2.867, gas fraction, α_g : 0.62

(a) SCMC-phase

(b) air-phase

Fig. 12. Contours of volume fraction for 90^0 elbow
SCMC concentration (kg/m^3): 0.8, SCMC velocity (m/s): 1.733, gas velocity (m/s): 2.3933, gas fraction, α_g : 0.58

(a) SCMC–phase and (b) air-phase

Fig. 13 shows that comparison plot of experimental results with CFD simulated results at different elbow angles. In both cases experimental results matches well with the CFD simulated results.
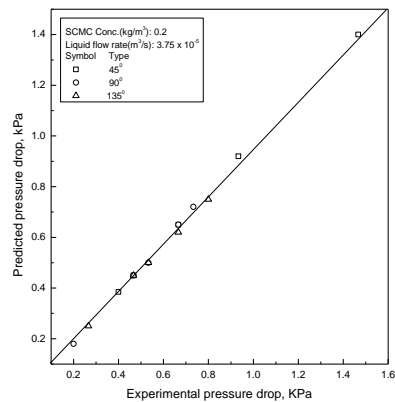

Fig. 13. Comparison of experimental results with CFD simulated results at different elbow angle

The flow pattern is depended on the flow rate of each phase, their interactions the transport properties and the geometry of the elbows. The flow regime was difficult to determine in the two-phase region. In general an accumulation of air towards the inside of the wall, this originates from the start of the elbow. This could be caused by a radial pressure gradient generated by the lower density mixture causing the slow-moving liquid phase near the wall to move toward the inside wall of the elbow. Phenomenon at high gas flow rates was observed by (Banerjee *et al.* 1967; Farukhi and Parker 1974; Maddock *et al.* 1974 and Usui *et al.* 1983).

5. CONCLUSIONS

1.   Computational Fluid Dynamics (CFD) analysis has been reported for non-Newtonian and gas-non-Newtonian liquids flow through different elbows in the horizontal plane. In all the cases the CFD modeling matches well with the experimental results as published earlier.

2.   In case of non-Newtonian liquid flow through elbows the CFD analysis predicts

i.   The velocity and pressure field at different points in the elbows,

ii.   The maximum velocity is shifted towards the inner wall of the elbow. The pressure is greatest at the outer wall furthest from the centre of curvature and least at the inner wall nearest to the centre of curvature. This is due to centrifugal forces.

3.   In case of gas-non-Newtonian liquid flow through elbows the CFD analysis predicts

i.   Velocity and pressure field at different points in the elbows for air-SCMC mixture and individual phases,

ii.   As the mixture enters to the elbows due to centrifugal action heavier density phase that is liquid moves to the outer wall and lower density phase, air moves to the inner wall. The static pressure profile of elbows show that for 45° elbow pressure drop is more comparing to the 135° elbow. Static pressure is high at outer wall as heavier density SCMC phase goes to outer wall due to centrifugal force and low at the inner wall when the air phase exits.

iii.   Contour plot of volume fraction show that heavier density SCMC phase goes to outer wall side and lighter air goes to inner wall side.

REFERENCES

Bandyopadyay, T. K. and Das, S. K., (2007). Non-Newtonian pseudoplastic liquid flow through small diameter piping components, *J. Petrol. Sc. & Engg.,* 55, 156-166.

Bandyopadyay, T. K., Banerjee T. K. and Das, S. K., (2000). Gas-non-Newtonian liquid flow through elbows, *Chem. Engg. Comm.*, 182(1), 21-33.

Banerjee, S., Rhodes, E. and Scott, D. S., (1967). Film inversion of concurrent two-phase flow in Helical coils, *AIChE J.*, 13(1), 189-191.

Banerjee, T. K. and Das, S. K., (1998). Gas-non-Newtonian liquids flow through globe and gate valves, *Chem. Engg. Comm.*, 167, 133-146.

Banerjee, T. K., Das, M. and Das, S. K., (1994). Non-Newtonian liquid flow through globe and gate valves, *Can. J. Chem. Engg.*, 72, 207-211.

Berrouk, A. B. and Laurence, D., (2008). Stochastic modeling of aerosol deposition for LES of 90^0 bend turbulent flow, *Int. J. Heat and Fluid Flow*, 29, 1010-1028.

Brown, Gary, (2006). Use of CFD to predict and reduce erosion in an Industrial slurry piping system, *5th Int. Conf. on CFD in the process industries CSIRO*, Melbourne, Australia, 13-15 December.

Das, S. K., Biswas, M. N. and Mitra, A. K., (1989). Pressure losses in Two-phase Gas-non-Newtonian liquid flow in horizontal tube, *J. Pipelines*, 7, 307-325.

Das, S. K., Biswas, M. N. & Mitra, A. K., (1991). Non-Newtonian liquid flow in bend, *Chem. Eng. J.*, 45, 165-171.

Edwards, M. F., Jadallah, M. S. M. and Smith, R., (1985). Head losses in pipe fittings at low Reynolds numbers, *Chem. Eng. Res. Dev.*, 63, 43-50.

Edwards, J. K., McLaury, B. S. and Shirazi, S. A., (1998). Supplementing a CFD code with erosion prediction capabilities, In *Proc. of ASME FEDSM'98: ASME Fluids Engineering Division Summer Meeting*, Washington D.C., June, 245, pp. 1-7.

Etemad, S. and Sunden, S., (2004). Numerical analysis of turbulent convective heat transfer processes in a square-sectioned U-bend duct, *15th Australasian Fluid Mechanics Conf.*, Sydney, Australia, 13-17 Dec.

Farukhi, Nayeem, M. and Parker, J. D., (1974). A visual study of air-water mixtures flowing inside Serpentine tubes, *Proceeding of the 5th International Conference, JSME*, Tokyo, B5.5, 205-209.

Fluent Users Guide, Version 6.3, Fluent India, Pune (2008).

Hidayat, M. and Rasmuson, A., (2002). Numerical investigation of gas-solid flow in a U-bend, *Proc. 13th Int. Drying Sym.*, **A**, Bejing, China, IDS' 424-433.

Kuan, B., Yang, W. and Solnordal, C., (2003). CFD simulation and experimental validation of dilute particulate turbulent flows in a 900 duct bend, 3rd *Int. Conf. on CFD in the Minerals and Process Industries CSIRO*, Melbourne, Australia 10-12 December.

Kumar, A., Kaushal, D. R. and Kumar, U., (2008). Bend Pressure drop experiments compared with Fluent, *Eng. Computational Mech.,* 161, 35-42.

Maddock, C., Lacey, P. M.C. and Patrick, M. A., (1974). The structure of two-phase flow in a curved pipe, *J. Chem., Engg. Synp. Series*, 38, 1-22.

Manzar, M. A. and Shah, S. N., (2009). Particle distribution and erosion during the flow of Newtonian and non-newtonian slurries in straight and coiled pipes, *Engg. Applications Comp. Mech.*, 3, 296-320.

Marn, J. and Ternik, P., (2006). Laminar flow of a shear-thickening fluid in a 90° pipe bend, *Fluid Dynamics Res.*, 38, 295-312.

Shah, N. S. and Jain, S., (2008). Coiled tubing erosion during hydraulic fracturing slurry flow, *Wear*, 264, 279-290.

Usui, K., Akoi, S. and Inoue, A., (1983). Flow behavior and phase distribution in two-phase flow around inverted U-bend, *J. Nucl. Sci. Technol.,* 20(11), 33-46.

Wu, B. and Chen, S., (2008). CFD simulation of non-Newtonian fluid flow in anaerobic digesters, *Biotecnol. Bioeng*. 99, 700-711.

Xia, B. and Sun, D. W., (2002). Applications of computational fluid dynamics (CFD) in the food industry: a review, *Comp.Eelec. Agriculture*, 34, 5-24.

Zhang, P., Gros, Y., Roberts, R. M. and Benard, A., (2010). Modeling of turbulent flow with particle deposition in curved pipes, *Proc. 7th Int. Conf. on Multiphase flow ICMF 2010*, Tampa, FL USA, May 30-June 4.